ACSNANO

www.acsnano.org

ARTICLE

Molecular Engineering of Pericellular Microniche *via* Biomimetic Proteoglycans Modulates Cell Mechanobiology

Elizabeth R. Kahle, Biao Han, Prashant Chandrasekaran, Evan R. Phillips, Mary K. Mulcahey, X. Lucas Lu, Michele S. Marcolongo,* and Lin Han*

Cite This: *ACS Nano* 2022, 16, 1220−1230

Read Online

ACCESS | Metrics & More | Article Recommendations

ABSTRACT: **Molecular engineering of biological tissues using synthetic mimics of native matrix molecules can modulate the mechanical properties of the cellular microenvironment through physical interactions with existing matrix molecules, and in turn, mediate the corresponding cell mechanobiology. In articular cartilage, the pericellular matrix (PCM) is the immediate microniche that regulates cell fate, signaling, and metabolism. The negatively charged osmo-environment, as endowed by PCM proteoglycans, is a key biophysical cue for cell mechanosensing. This study demonstrated that biomimetic proteoglycans (BPGs), which mimic the ultrastructure and polyanionic nature of native proteoglycans, can be used to molecularly engineer PCM micromechanics and cell mechanotransduction in cartilage. Upon infiltration into bovine cartilage explant, we showed that localization of BPGs in the PCM leads to increased PCM micromodulus and enhanced chondrocyte intracellular calcium signaling. Applying molecular force spectroscopy, we revealed that BPGs integrate with native PCM through augmenting the molecular adhesion of aggrecan, the major PCM proteoglycan, at the nanoscale. These interactions are enabled by the biomimetic "bottle-brush" ultrastructure of BPGs and facilitate the integration of BPGs within the PCM. Thus, this class of biomimetic molecules can be used for modulating molecular interactions of pericellular proteoglycans and harnessing cell mechanosensing. Because the PCM is a prevalent feature of various cell types, BPGs hold promising potential for improving regeneration and disease modification for not only cartilage-related healthcare but many other tissues and diseases.**

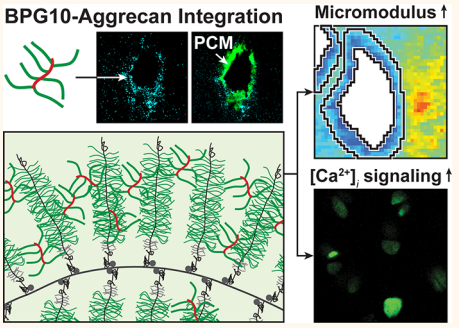

KEYWORDS: *biomimetic proteoglycan, pericellular matrix, chondrocyte mechanotransduction, nanomechanics, articular cartilage*

Over the past decades, there has been increasing appreciation of the biophysical and biomechanical cross-talk between the extracellular matrix (ECM) and residing cells.[1−3] In particular, the immediate cell microenvironment plays a pivotal role in regulating mechano-sensitive cellular activities such as adhesion,[4] migration,[5] solute transport,[6] mechanotransduction,[7] and metastasis.[8] In turn, owing to its immediate contact with cells, the microniche is often the initiation point of disease onset, contributing to disrupted cell mechanobiology and more widespread tissue degeneration.[9] This immediate cell microniche thus emerges as a promising therapeutic target for modulating cell mechano-transduction, detecting, or ameliorating early disease onset as well as improving tissue regeneration.[10,11]

For many tissue types, the immediate cell microniche, termed the "pericellular matrix (PCM)" or "glycocalyx layer", has distinct composition and structure relative to the bulk ECM. Examples include articular cartilage,[12] meniscus,[13] intervertebral disc,[14] injured tendon,[15] endothelium,[16] stem cell niche,[17] and solid tumors.[8] This microenvironment is characterized by exclusive localization or a preferred distribution of proteoglycans and proteoglycan−hyaluronan (HA) complexes.[12,18] These proteoglycans have a wide spectrum of interactions with cell surface receptors, growth factors, and cytokines, and thus, play key roles in mediating cellular metabolism, signaling, and cell-matrix cross-talk.[19] Additionally, they endow cells with a highly negatively charged environment, a key biophysical cue governing cell mechano-

Received: October 12, 2021
Accepted: January 7, 2022
Published: January 11, 2022

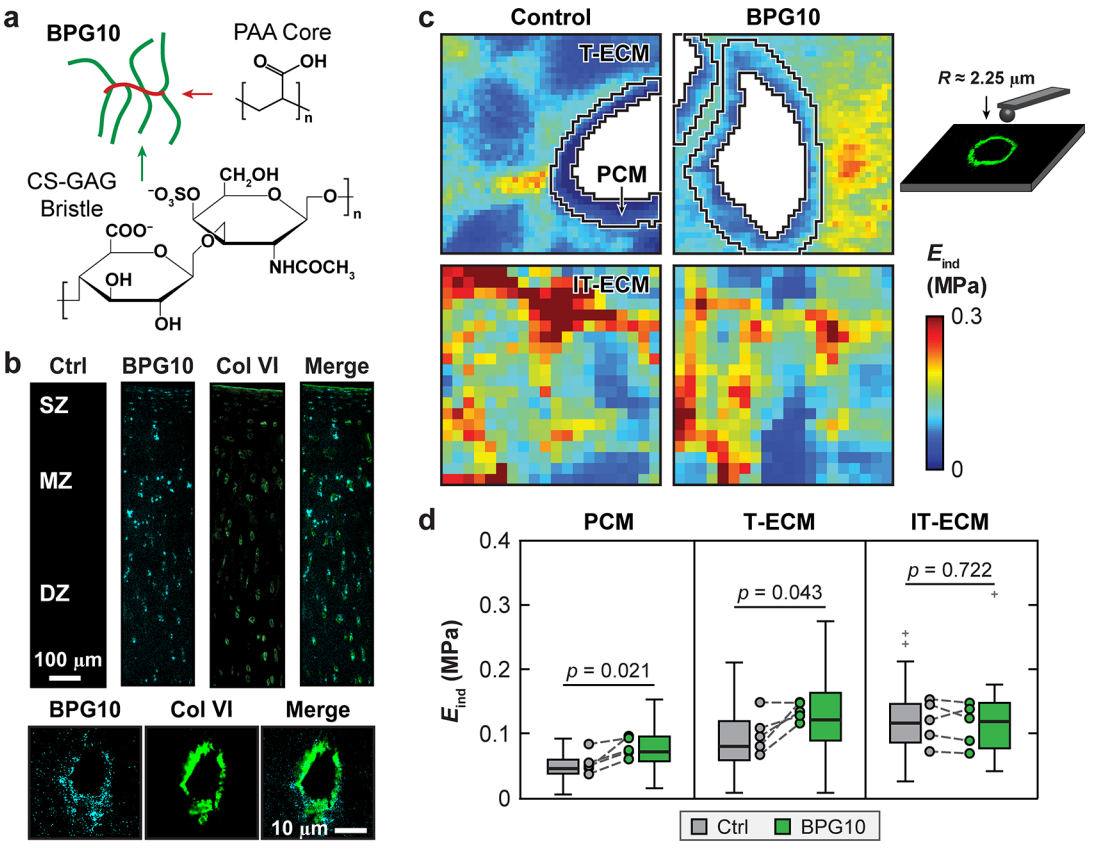

Figure 1. Localization of BPG10 in cartilage pericellular matrix (PCM) augments the micromechanics of PCM. (a) Molecular architecture of BPG10, containing ~7 CS-GAG side chains (schematic shown for chondroitin-4-sulfate GAG) conjugated to the PAA backbone. (b) Immunofluorescence (IF) images of adult bovine cartilage explants infiltrated with fluorescently labeled BPG10 and co-stained with collagen VI demonstrate the diffusion of BPG10 throughout all zones of the tissue (SZ, superficial zone; MZ, middle zone; DZ, deep zone) and preferred distribution within the PCM and nearby territorial domain (T-ECM). (c) (left panel) Representative indentation modulus (E_{ind}) maps of control and BPG10-treated cartilage in 20 × 20 μm^2 regions of interest (ROIs) either containing well-defined PCM rings (40 × 40 indents) or interterritorial domains (IT-ECM) further removed from cells (20 × 20 indents). Moduli corresponding to cell remnants were removed (white voids). (right panel) Schematic illustration of IF-guided AFM nanomechanical mapping on bovine cartilage cryosections using a microspherical tip ($R \approx 2.25\ \mu m$), the PCM is immunolabeled with collagen VI. (d) Box-and-whiskers plots of the PCM, T-ECM, and IT-ECM micromodulus for control and BPG10-treated cartilage (>600 locations for each region, n = 5 animals). Each matched pair of circles represents the average modulus of untreated and BPG10-treated cartilage of the same animal.

sensing *in vivo*.[20] However, given their high susceptibility to catabolic enzymes, degradation of proteoglycans upon disease onset often precedes that of other matrix constituents, such as collagens,[21] rendering proteoglycans an emerging target for restoring cell microniche integrity and modifying disease progression. Indeed, many efforts have been dedicated to developing proteoglycan-based biomedicine. These studies have primarily focused on exploiting the biological functions using either native proteoglycans or biomimetic proteoglycan constructs that recapitulate their biological binding activities.[22] In contrast, there have been very limited attempts in modulating the biophysical and mechanobiological roles of proteoglycans in the pericellular microniche.

This proof-of-concept study aims to demonstrate that biomimetic proteoglycans (BPGs), which mimic the nanoscale architecture of native proteoglycans, can be used to molecularly engineer the pericellular microniche, thereby modulating cell mechanosensitive activities in a minimally invasive approach. Here, we used articular cartilage as the model system, as the PCM of cartilage has been studied extensively,[10,12] allowing us to pinpoint the molecular mechanisms of BPGs in engineering the PCM. Cartilage PCM is characterized by exclusive localization of type VI collagen,[23] perlecan,[24] and biglycan.[25] Aggrecan, the major proteoglycan of cartilage matrix, is also preferentially localized in the PCM.[26] *In vivo*, aggrecan undergoes faster turnover in the PCM than in the bulk matrix,[27] with newly synthesized aggrecan primarily localized therein.[28] Aggrecan has a "bottle-brush"-like ultrastructure, with a ~400 nm core protein decorated with ~100 densely packed, 40 nm long chondroitin sulfate glycosaminoglycan (CS-GAG) side chains and a few shorter keratan sulfate (KS)-GAGs.[29] The fixed negative charges on CS-GAGs of aggrecan are the primary determinant of cartilage osmotic environment and PCM-mediated chondrocyte mechanosensing.[30] Recently, we have synthesized BPGs by conjugating CS-GAGs onto a poly(acrylic acid) (PAA) synthetic backbone.[31−33] BPGs partially mimic the bottle-brush nanostructure and polyanionic nature of native aggrecan. Here, we tested the capability of the BPGs in modulating chondrocyte mechanotransduction behaviors *in situ*. Our results show that BPGs can integrate with native cartilage PCM through molecular adhesion interactions with the residing aggrecan. In doing so, BPGs can augment the PCM micromechanics and chondrocyte mechanotransduction,

https://doi.org/10.1021/acsnano.1c09015
ACS Nano 2022, 16, 1220−1230

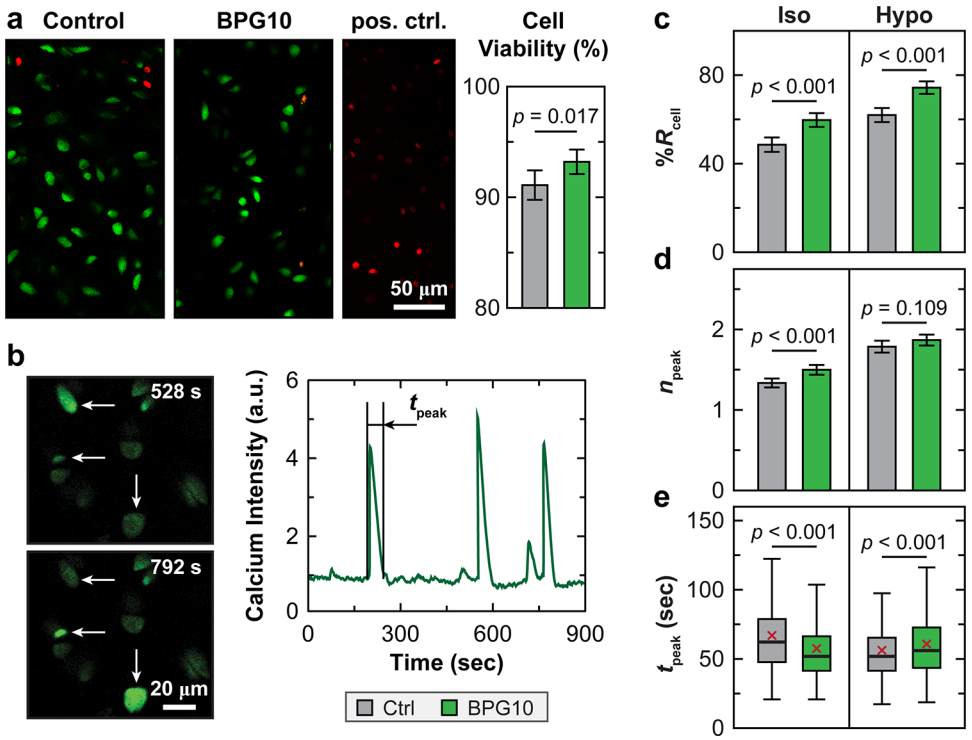

Figure 2. Infiltration of BPG10 into bovine cartilage explants promotes intracellular spontaneous calcium signaling, $[Ca^{2+}]_i$, activities of chondrocytes *in situ*. (a) Representative cell live/dead assay images of control and BPG10-treated adult bovine cartilage after 24 h exposure, with methanol-treated, devitalized cartilage as internal positive control. Cell viability is quantified on ≥1750 cells per treatment from n = 3 animals (mean ± 95% CI). (b) Representative confocal images of chondrocyte $[Ca^{2+}]_i$ signaling and corresponding $[Ca^{2+}]_i$ oscillation intensity curve of a single cell over a 15 min time frame illustrating the definition of t_{peak}. Chondrocytes were labeled with Cal-520^{AM} and time series images were recorded using a confocal microscope with a 20× objective submerged in DMEM at 37 °C. (c−e) Comparison of $[Ca^{2+}]_i$ signaling characteristics between BPG10-treated and control cartilage explants in both isotonic and hypotonic media: (c) percentage of responding cells, $\%R_{cell}$ (mean ± 95% CI), (d) number of peaks within the 15 min testing time frame, n_{peak} (mean ± 95% CI), and (e) duration of each peak, t_{peak} (box-and-whisker plot, outliers are not shown to increase clarity, red cross represents the mean value). Data represent ≥445 responding cells pooled from n = 3 animals for each group.

thereby enabling us to molecularly engineer cartilage *via* a minimally invasive strategy for potential osteoarthritis treatment.

RESULTS

Of our suite of synthesized BPGs, we used BPG10 as the model biomimetic proteoglycan. BPG10 consists of a ∼10 kDa synthetic PAA core, decorated with ∼5−7 CS-GAG bristles (Figure 1a). The focus of BPG10 here was due to its capability of effectively diffusing into cartilage following intra-articular injection into rabbit knees *in vivo*[34] or after 24 h incubation of human or bovine explants in BPG10 aqueous solution *in vitro*.[35] Also, similar to aggrecan, BPG10 exhibits the "bottle-brush" architecture, with CS-GAGs packed at 3−4 nm spacing along the PAA core,[31] comparable to the 2−3 nm spacing of CS-GAGs along aggrecan core protein,[36] indicating that BPG10 may partially mimic the biophysical characteristics of native aggrecan. After immersion of normal adult bovine cartilage explants in 10 mg/mL fluorescently labeled BPG10 for 24 h, we investigated the colocalization of BPG10 and collagen VI, one key biomarker of cartilage PCM.[23] BPG10 was found to be more concentrated in the PCM, with reduced concentration in the territorial domain of ECM (≤10 μm from the PCM outer rim, or the T-ECM). In the bulk of ECM that is further removed from cells, or the interterritorial domain (IT-ECM), we did not detect appreciable fluorescent signal of BPG10, indicating its low presence in this region (Figure 1b).

To determine the impact of BPG10 localization on PCM micromechanics, we applied immunofluorescence (IF)-guided AFM nanomechanical mapping[9,37] on unfixed, sagittal cryosections of bovine cartilage after 24 h immersion in 10 mg/mL BPG10 *versus* the untreated control. In brief, immediately following BPG10 diffusion, 8 μm thick, unfixed cryosections of bovine cartilage were prepared *via* the Kawamoto's film-assisted cryosectioning.[38] We performed the nanomechanical mapping on 20 × 20 μm^2 regions with well-defined PCM rings and then separated the micromoduli of PCM and its nearby T-ECM based on the IF-labeling of collagen VI (Figure 1c). The tests were also performed in 20 × 20 μm^2 regions further removed from the PCM and cells, which represent the IT-ECM, or the bulk matrix. Infiltration of BPG10 was found to significantly increase the PCM micromodulus (79 ± 13 kPa) by 53 ± 32% (mean ± 95% CI, n = 5, p = 0.021) relative to the untreated control (54 ± 16 kPa). Meanwhile, the territorial domain (T-ECM) also exhibited an increase of the micromodulus (44 ± 32%, p = 0.043) (Figure 1d). In contrast, we did not detect marked changes in the micromodulus of the IT-ECM after BPG10 infiltration (Figure 1c,d). These changes in the local micromodulus corroborate the preferred distribution of BPG10 in the PCM (Figure 1b) and clearly illustrate BPG10's capability in augmenting the chondrocyte microenvironment without substantially altering the bulk matrix (IT-ECM) properties.

https://doi.org/10.1021/acsnano.1c09015
ACS Nano 2022, 16, 1220−1230

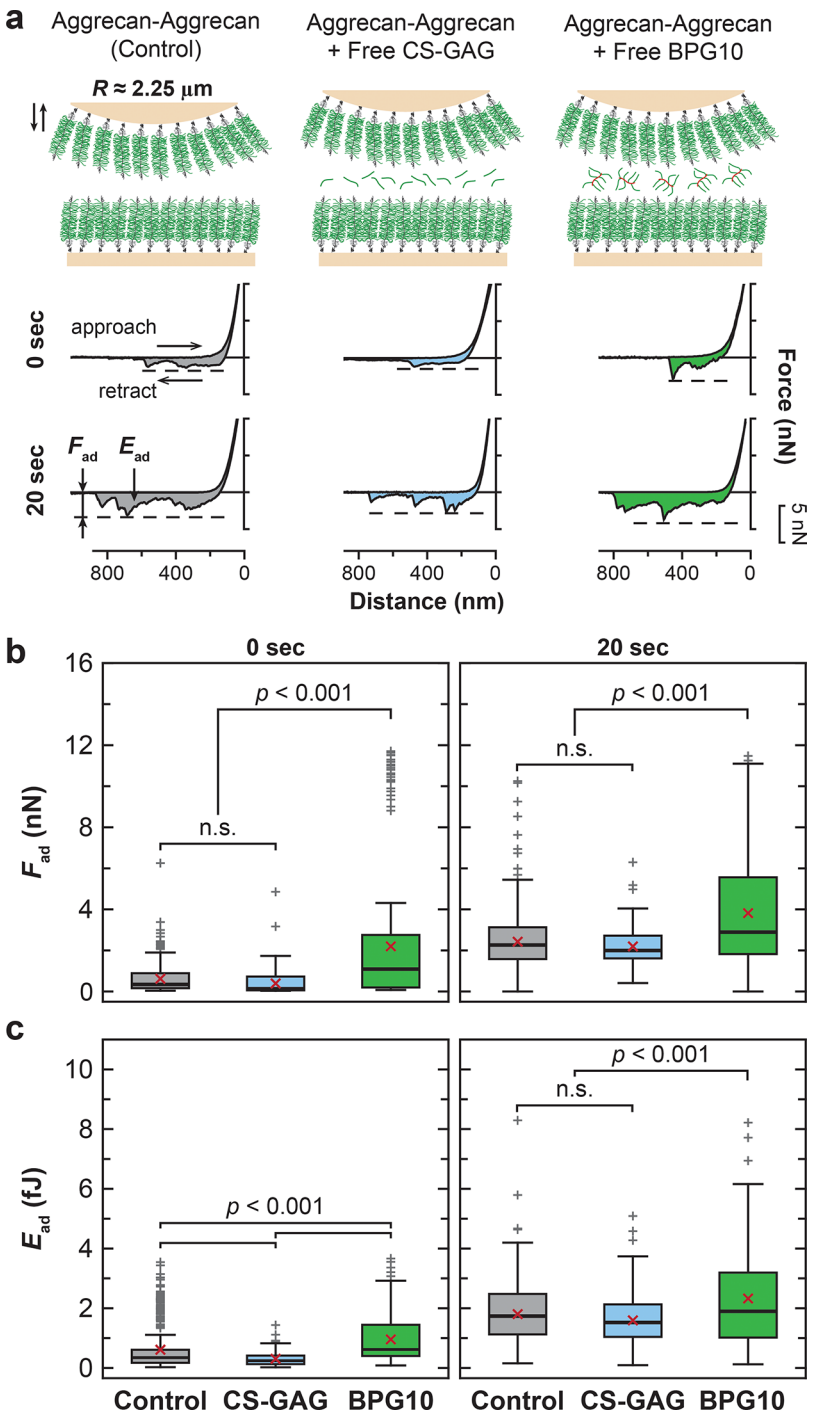

Figure 3. BPG10 increases the molecular adhesion of aggrecan. (a) Colloidal force spectroscopy for the measurement of molecular adhesion between opposing aggrecan−aggrecan molecules in 1× PBS (control) or 1× PBS with the addition of free CS-GAGs at 3.3 μg/mL or free BPG10 at 3.5 μg/mL. (top panels) Schematic illustration of experimental setup. (bottom panels) Representative force−distance curves illustrate the long-range adhesion behaviors between opposing aggrecan molecules at both 0 and 20 s dwell time, as well as the definition of maximum adhesion force, F_{ad}, and total adhesion energy, E_{ad}. (b,c) The addition of free BPG10 significantly increases (b) F_{ad}, and (c) E_{ad}, between aggrecan−aggrecan molecules at both 0 and 20 s dwell times. In comparison, addition of free CS-GAG does not have a significant impact, except for a mild decrease in F_{ad} at 0 s dwell time ($n \geq 180$ measurements from three technical repeats for each condition, red cross represents the mean value).

Given the pivotal role of PCM in mediating cell−matrix interactions, we next queried the effects of BPG10 on chondrocyte viability and mechanotransduction *in situ*. Using the live/dead assay, we found that infiltration of BPG10 had only a marginal impact on cell viability (1.93 ± 1.90% increase relative to the control, $p = 0.017$), demonstrating minimal cellular toxicity (Figure 2a). We then studied the intracellular calcium signaling, $[Ca^{2+}]_i$, activities of cartilage explants in both physiological (isotonic) and osmotically instigated (hypotonic) Dulbecco's Modified Eagle Medium (DMEM). For both BPG10-treated and untreated controls, we observed spontaneous $[Ca^{2+}]_i$ oscillations (Figure 2b) from which we

https://doi.org/10.1021/acsnano.1c09015
ACS Nano 2022, 16, 1220−1230

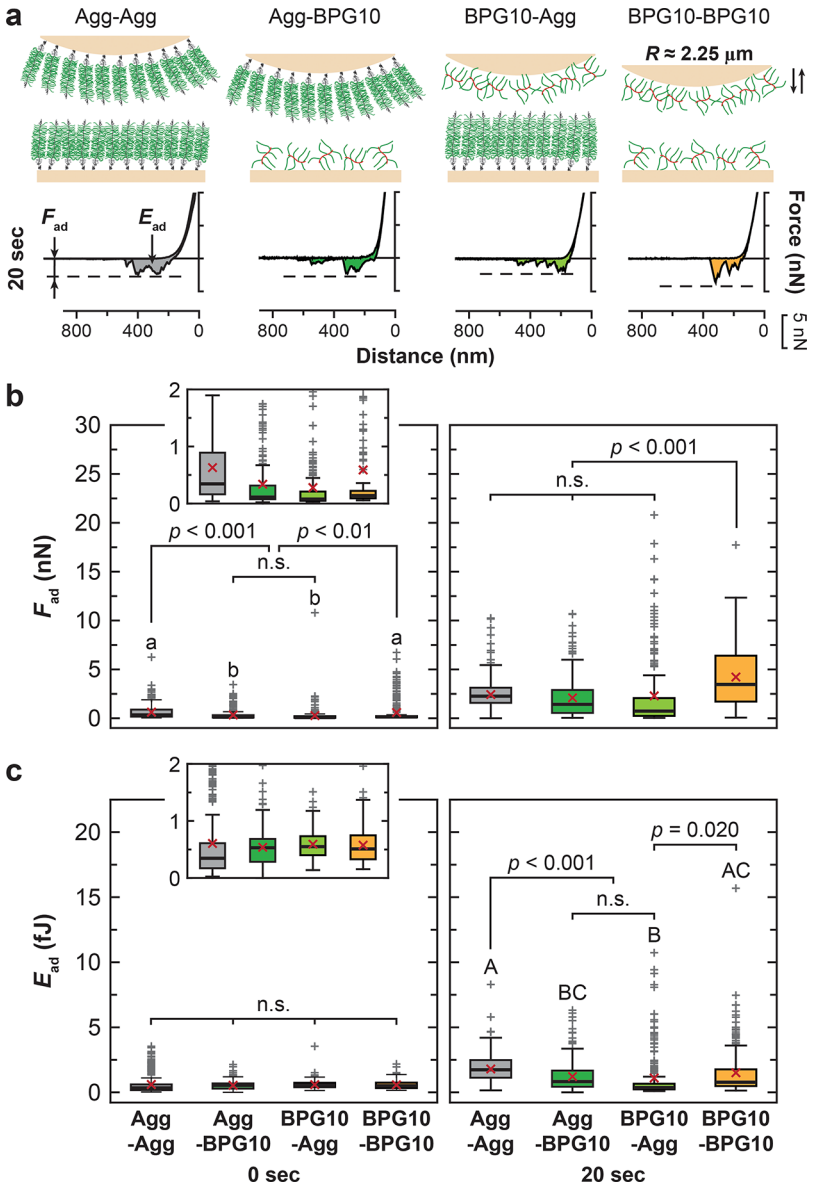

Figure 4. Comparison of molecular adhesion interactions between BPG10 and aggrecan. (a) Colloidal molecular force spectroscopy for the measurement of molecular adhesion between BPG10−aggrecan molecules (aggrecan-coated tips *versus* BPG10-coated substrates, BPG10-coated tips *versus* aggrecan-coated substrates), and between BPG10-BPG10 molecules in 1× PBS. (top panels) Schematic illustration of experimental setup. (bottom panels) Representative force−distance curves illustrate the long-range adhesion behaviors between aggrecan−aggrecan, BPG10−aggrecan, and BPG10−BPG10 at 20 s dwell time. (b,c) Comparison of (b) maximum adhesion force, F_{ad}, and (c) total adhesion energy, E_{ad}, between aggrecan−aggrecan, BPG10−aggrecan, and BPG10−BPG10 molecules in 1× PBS. Insets illustrate the zoom-in comparisons of F_{ad} and E_{ad} at 0 s dwell time. At 0 s dwell time, BPG10−aggrecan interactions yield lower F_{ad} but similar E_{ad} relative to aggrecan−aggrecan and BPG10−BPG10 interactions. At 20 s dwell time, BPG10−aggrecan interactions show similar F_{ad} but lower E_{ad} relative to aggrecan−aggrecan interactions, as well as lower F_{ad} and mildly lower E_{ad} relative to BPG10−BPG10 interactions ($n \geq 190$ measurements from three technical repeats for each condition, red cross represents the mean value). Different letters indicate significant differences between groups. Data of aggrecan−aggrecan adhesion are replotted from the control experiment from Figure 3.

extracted the temporal parameters including the percentage of responding cells, $\%R_{cell}$, the total number of $[Ca^{2+}]_i$ peaks, n_{peak}, and the average duration of peaks, t_{peak}, from each responding cell over a 15 min observation period. In isotonic DMEM, BPG10 treatment significantly enhanced the *in situ* $[Ca^{2+}]_i$ activities, as marked by increased $\%R_{cell}$, n_{peak}, and reduced t_{peak} (Figure 2c−e). In hypotonic DMEM, the electrical double layer (EDL) repulsion between sGAGs is amplified, resulting in increased compressive strain on ECM constituents[39] as well as residing chondrocytes,[40] similar to the case of physiologic joint compression. Under this osmotically instigated condition, as expected, chondrocytes exhibited enhanced $[Ca^{2+}]_i$ activities relative to the isotonic condition for both groups. Meanwhile, the BPG10-treated group also showed increased $\%R_{cell}$ but had no changes in n_{peak} and only a mild increase in t_{peak} relative to the control (Figure 2c−e). Collectively, our results showed that localization of BPG10 in the PCM augments chondrocyte mechanosensing of its native microenvironment under both physiological and osmotically stimulated conditions.

In native cartilage ECM, aggrecan adapts a highly compressed conformation, with ∼50% molecular compressive

https://doi.org/10.1021/acsnano.1c09015
ACS Nano 2022, 16, 1220−1230

strain in unloaded tissue.[41] This densely packed aggrecan moiety endows cartilage with its specialized load bearing and energy dissipation functions.[29] Given the higher concentration of aggrecan in the PCM, it may seem counterintuitive that BPG10, which also possesses fixed negative charges, can diffuse throughout the negatively charged matrix and localize within the PCM. However, we have previously shown that in a cartilage matrix, despite the presence of strong EDL repulsion, aggrecan can undergo self-adhesion under its highly compressed conformation, which is enabled by its "bottle-brush"-like ultrastructure and contributes to its retention *in vivo*.[42] We thus investigated if BPG10 also exhibits similar adhesion behaviors with aggrecan by applying AFM molecular force spectroscopy to two opposing layers of aggrecan biomimetic assemblies *in vitro* at near-physiological packing densities (∼50 mg/mL), following the established procedure.[42,43] Magnitude of adhesion, as characterized by the maximum adhesion force, F_{ad}, and total adhesion energy, E_{ad}, was quantified after holding the compression of two aggrecan layers at their physiological strain in unloaded cartilage (∼50%)[41] in 1× PBS for 0 and 20 s, respectively (Figure 3a). In comparison to the control system without BPG10, addition of free BPG10 to the solution was found to significantly increase both E_{ad} and F_{ad} at both 0 and 20 s equilibration durations (Figure 3b,c). These results evidenced the capability of BPG10 to undergo molecular adhesion with aggrecan, thereby forming molecular complexes with the aggrecan networks and strengthening its integration with the native matrix. In contrast, when CS-GAGs were added to the solution at a CS-GAG concentration equivalent to that of BPG10, we did not detect appreciable changes in aggrecan−aggrecan adhesion, except for a mild decrease in F_{ad} at 0 s equilibration. Thus, the increased adhesion by BPG10 could be endowed by its "bottle-brush"-like, aggrecan-mimicking nanostructure.

Next, we quantified the magnitude of BPG10−BPG10 and BPG10−aggrecan molecular interactions. We constructed the biomimetic assembly of BPG10 through chemical attachment onto gold-coated planar substrates and colloidal AFM tips (Figure 4a). We then measured the adhesion between opposing layers of BPG10−aggrecan and BPG10−BPG10 in 1× PBS and compared the results with aggrecan−aggrecan adhesion measured in the absence of free BPG10 or CS-GAG (Figure 3). For BPG10−aggrecan interactions, we tested the adhesion between both aggrecan-coated tips *versus* BPG10-coated planar substrates and between BPG10-coated tips *versus* aggrecan-coated substrates (Figure 4a). These two experiments yielded similar F_{ad} and E_{ad} at both 0 and 20 s equilibration durations (Figure 4b,c), confirming the consistency and repeatability of the biomimetic assembly of BPG10. For all four cases, the magnitudes of F_{ad} and E_{ad} were relatively low at 0 s equilibration, but substantially increased at 20 s. Comparing the four cases, BPG10−BPG10 interactions showed higher F_{ad} (4.22 ± 0.44 nN, mean ± 95% CI, $p < 0.001$) than those of aggrecan−aggrecan (2.42 ± 0.15 nN) and BPG10−aggrecan (2.10 ± 0.26 nN by aggrecan-coated tips, 2.30 ± 0.52 nN by BPG10-coated tips) (Figure 4b). On the other hand, the magnitudes of E_{ad} were similar across these conditions, except for a moderately lower adhesion between BPG10−aggrecan (1.22 ± 0.15 fJ by aggrecan-coated tips, 1.10 ± 0.26 fJ by BPG10-coated tips) in comparison to aggrecan−aggrecan (1.80 ± 0.10 fJ) and BPG10−BPG10 (1.51 ± 0.24 fJ) (Figure 4c). Taken together, these results indicate that BPG10 can undergo direct adhesion interactions with aggrecan molecules, with an adhesion energy at a similar magnitude as that of aggrecan−aggrecan self-adhesion. In addition, similar to native aggrecan, BPG10 can undergo self-adhesion, which could result in a physically interconnected network of BPG10 molecules that are integrated with the aggrecan network, thereby increasing the stability and retention of BPG10 in the PCM microenvironment.

DISCUSSION

This study demonstrates biomimetic proteoglycans as a promising molecular therapy target for engineering the PCM micromechanics (Figure 1) and cell mechanotransduction (Figure 2) through interactions with native aggrecan (Figures 3 and 4). These findings indicate that BPGs can potentially be used for improving tissue engineering of cartilage and possibly other load-bearing tissues as well. When chondrocytes, without their PCM, are cultured *in vitro*, a soft hydrogel (<10 kPa) is required for maintaining cell viability and preventing dedifferentiation.[44] *In vivo*, however, despite being surrounded by the native PCM that is much stiffer (∼50 kPa in human,[45] ∼1 MPa in mice[30]), residing chondrocytes are able to maintain their phenotype and metabolic activities. This highly negatively charged osmotic microenvironment, as endowed by aggrecan in the PCM, is a crucial biophysical cue for chondrocyte mechanosensing, as loss of the PCM fixed charges leads to markedly demoted chondrocyte $[Ca^{2+}]_i$ activities *in situ*.[30] Although outcomes of active $[Ca^{2+}]_i$ signaling do not reveal direct downstream biological pathways, these parameters are positively correlated with chondrocyte anabolism,[46] pointing to a key role of PCM in regulating cell phenotype and metabolic homeostasis. To this end, the capability of BPG10 to enhance $[Ca^{2+}]_i$ activities in both physiological (isotonic) and osmotically instigated (hypotonic) environments (Figure 2c−e) suggests that its localization in the PCM can modulate chondrocyte mechanosensing. Thus, BPG10 may promote chondrocyte biosynthesis and cartilage regeneration, either alone or in combination with other biomechanical stimuli. In osteoarthritis, loss of PCM mechanical integrity and demotion of chondrocyte $[Ca^{2+}]_i$ activities are among the earliest events of disease initiation, preceding histological damage or loss of overt tissue biomechanical functions.[9,47,48] BPG10 could thus be used to restore the osmo-environment in degenerative cartilage, thereby alleviating the disruption of chondrocyte mechanotransduction and degradation of cartilage. Because the synthetic PAA core of BPG10 does not contain peptide sequences susceptible to catabolic enzymes (Figure 1a),[31] BPG10-based therapy has the potential to achieve robust rescue outcomes by resisting aggravated enzymatic catabolism.

The function of BPG10 in molecularly engineering the PCM arises from its interactions with aggrecan. One key biophysical characteristic of cartilage matrix is the high degree of nanoscale heterogeneity in the electrical potential.[49,50] Within cartilage, the Debye length, κ^{-1}, which characterizes the exponential decay distance of EDL repulsion effect, is ∼ 1 nm,[51] of the same order as the CS-GAG packing distance along aggrecan core protein (∼ 2−3 nm).[36] As a result, the electrical potential is highly heterogeneous, and thus, the EDL interactions within the tissue can be quantitatively described by the unit cell model[49] or charged rod model[50] that account for the nanoscale heterogeneity but not the continuum Donnan model.[51] This heterogeneity not only determines the tissue-level compressive modulus but also contributes to the intermolecular interactions of aggrecan. *In vivo*, aggrecan undergoes molecular adhesions

https://doi.org/10.1021/acsnano.1c09015
ACS Nano 2022, 16, 1220−1230

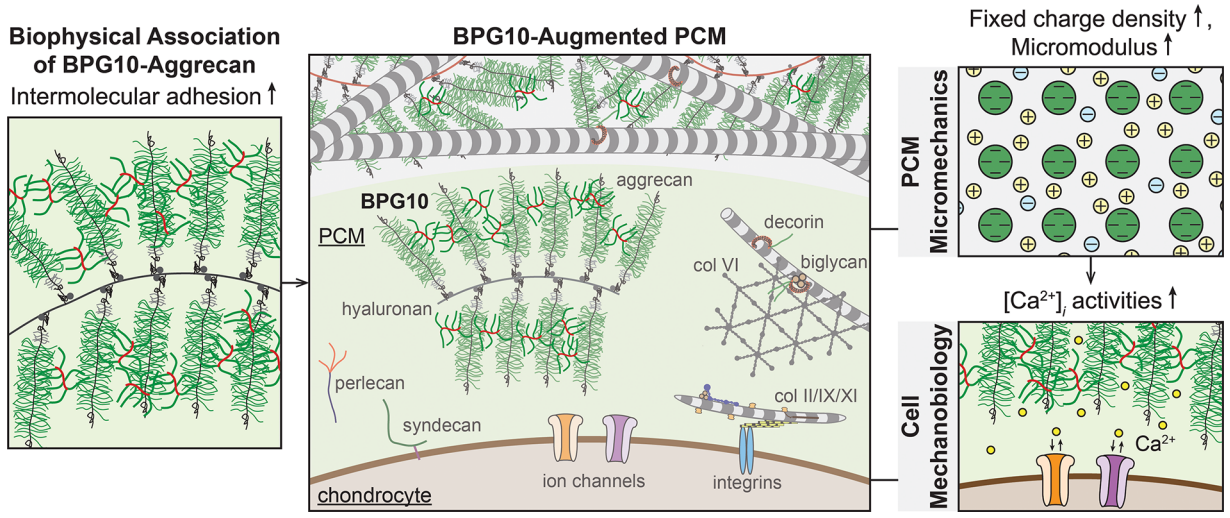

Figure 5. Schematic illustration of the working hypothesis of biomimetic proteoglycans in mediating pericellular microniche mechanics and cell mechanobiology. The biophysical adhesion interactions between BPG10 and aggrecan enables the integration of BPG10 with the aggrecan-enriched cartilage PCM, and thus, the preferred localization of BPG10 in the PCM. Such localization augments the micromechanical properties of cartilage PCM, and thus, promotes chondrocyte mechanotransduction. Therefore, BPG10 could potentially affect downstream cell signaling and metabolic activities through molecularly engineering the pericellular microniche.

with other aggrecan molecules, decorin, and collagen II fibrils, which are attributed to nonspecific interactions such as hydrogen bonding, Ca^{2+}-mediated ion bridging, van der Waals, and physical entanglement.[42,43,52] These interactions enhance the integration and retention of aggrecan−HA supramolecular aggregates within the porous collagen fibrillar network of cartilage matrix. BPG10, with CS-GAG bristles packed ∼3−4 nm apart along the PAA core (Figure 1), mimics not only the ultrastructure of aggrecan but also the heterogeneity of electrical potential therein. Therefore, similar to the case of aggrecan, BPG10 undergoes self-adhesion with other BPG10 molecules, which could lead to the formation of physically connected networks of BPG10. Additionally, BPG10 executes pronounced adhesion with aggrecan (Figure 4), possibly driven by physical interactions between the CS-GAGs of BPG10 and those of aggrecan *via* chain interpenetration and interdigitation.[53,54] This partially explains the preferential distribution of BPG10 in the PCM, where aggrecan is also more concentrated.[26] The association of BPG10 with aggrecan thus contributes to its preferred localization in the PCM. Given its negatively charged nature, the localized BPG10 increases the fixed charge density within the PCM microenvironment. In cartilage, Poisson−Boltzmann interactions arising from the fixed negative charges of aggrecan are the dominant factor of aggrecan compressive resistance[51] and a major determinant of the tissue modulus (∼50% of compressive modulus).[55] Thus, we hypothesize that when localized in the PCM, BPG10 not only directly increases the local fixed charge density and PCM micromodulus but provides additional physical linkages to enhance the integrity and stability of aggrecan network therein. In turn, this BPG10-augmented microniche promotes chondrocyte mechanosensitive activities (Figure 5).

The biomimetic "bottle-brush" nanostructure of BPG10 is crucial to its molecular functions. While free BPG10 increases aggrecan−aggrecan adhesion through providing additional physical linkages, individual CS-GAG chains do not have such effect (Figure 3). In comparison to BPG10, linear CS-GAGs do not possess the heterogeneous electrical field or the more complex architecture that provides the basis for increased molecular contact and entanglement. Therefore, interactions between CS-GAGs and aggrecan are possibly dominated by the EDL repulsion, which minimizes any potential adhesion interactions with aggrecan (Figure 3). Meanwhile, the more sparsely packed CS-GAG bristles on BPG10 experience weaker EDL repulsion than that of aggrecan. This could explain the higher adhesion force measured between BPG10−BPG10 than that of BPG10−aggrecan or aggrecan−aggrecan under near-physiological conditions (Figure 4b). On the other hand, given that the synthetic PAA core is shorter than aggrecan core protein, BPG10 also exhibits shorter interaction distances (Figure 4a). Collectively, the adhesion energy between BPG10−BPG10 is only mildly higher than that of BPG10−aggrecan (Figure 4c). Thus, by mimicking the structure of aggrecan, BPG10 is able to replicate the biophysical interactions of aggrecan with similar adhesion interaction magnitude, and thus, integrates with the native matrix.

The design of BPG10 primarily mimics the biophysical characteristics of proteoglycans, including the molecular structure and polyanionic nature. Given the absence of a protein core, we do not expect BPG10 to replicate specific biological binding activities of native proteoglycans like other peptide-based biomimetics.[56−58] Our primary focus is thus on the interactions between BPG10 and aggrecan, as well as its impact on tissue micromechanics and cell mechanotransduction. However, we do not rule out that BPG10 may also have other biological or biophysical roles by interacting with other quantitatively minor matrix constituents. For instance, the structure of BPG10 is also similar to that of perlecan, a PCM-specific heparan sulfate (HS) proteoglycan that contains three HS-GAG/CS-GAG chains.[59] In cartilage, perlecan is exclusively localized in the PCM,[24,60] where it regulates cell surface mechanosensing and activation of fibroblast growth factor (FGF)-2 signaling.[61] While BPG10 does not possess the same binding activities as perlecan, it may interact with perlecan in a manner similar to that of aggrecan, and thus, could influence the availability and bioactivity of perlecan. In addition, turnover of cartilage matrix involves endocytosis of HA in the PCM through CD44/HA receptors.[62] Binding of aggrecan

https://doi.org/10.1021/acsnano.1c09015
ACS Nano 2022, 16, 1220−1230

to HA in the PCM mediates this process by limiting CD44–HA interactions.[63] It is possible that BPG10 could also affect HA internalization by engineering the PCM molecular landscape.

Building on current findings, our future studies will investigate how BPG10 influences the activities of other matrix constituents and chondrocyte signaling, in addition to its marked impact on mechanotransduction (Figure 2). For instance, BPGs could be conjugated with small molecule growth factors or potential disease-modifying drugs using environmentally responsive, "smart" linkers, such as pH- or matrix metalloproteinase (MMP)-sensitive linkers.[64,65] BPGs could thus potentially serve as a carrier for facilitating the delivery of drugs to the PCM to promote cell anabolism or rescue degeneration. Furthermore, by modifying the synthesis conditions of BPGs, we can control the size of the synthetic core, as well as the type, number, density, and length of GAG side chains. For example, we have previously synthesized BPG250[32] and BPG0.5,[33] and each of these molecules has distinctive molecular architecture, which could endow specialized molecular interactions and cell mechanoresponses. *In vivo*, aggrecan exhibits marked variation in glycosylation and sulfation pattern, packing density, and length of CS-GAGs during development and aging, which contribute to age-associated cartilage maceration and increased susceptibility to OA.[66−68] Thus, our ongoing studies aim to modulate the molecular structure and composition of these biomimetic molecules and study the impacts of their interactions with native matrix molecules on the pericellular microniche integrity and cell mechanotransduction.

CONCLUSIONS

This study demonstrates the proof-of-concept that biomimetic proteoglycans can be used to molecularly engineer the pericellular microniche. By mimicking the "bottle-brush"-like ultrastructure and polyanionic nature of proteoglycans, we show that BPG10 can integrate with aggrecan in native cartilage through biophysical adhesions. These interactions contribute to the preferred localization of BPG10 in the PCM and lead to increased PCM micromodulus and enhanced chondrocyte $[Ca^{2+}]_i$ signaling (Figure 5). Given the pivotal role of PCM in cell-matrix interactions, our results provide a foundation for using biomimetic proteoglycans to harness cell mechanoresponses and modify disease progression. Notably, the negative charge-rich pericellular matrix is a prevalent feature in many tissue types, such as other musculoskeletal tissues,[13,14] stem cell niche,[17] and solid tumors,[8] and has been shown to play key roles in their homeostasis and pathogenesis. The applications of BPGs are thus not limited to articular cartilage and can be further extended to other tissues and diseases.

METHODS

Synthesis and Functionalization of BPG10. BPG10 was synthesized and fluorescently labeled, following established procedures.[31,32] Briefly, BPG10 was synthesized by reaction of commercial CS-GAG (~22 kDa, mixture of chondroitin-4-sulfate and chondroitin-6-sulfate GAGs, Sigma) in aqueous buffer and poly(acryloyl chloride) (PAC) (~10 kDa, in 25% dioxane, PolySciences) in ethyl acetate (Fisher Scientific) at a 1:10 CS:PAC molar ratio.[31] Fluorescently labeled BPG10 was synthesized by periodate oxidation of the CS-GAG chains of BPG10 and subsequent conjugation with 7-diethylaminocoumarin-3-carboxylic acid, hydrazide (DCCH, Sigma).[32] In addition, BPG10 was thiol-functionalized in a two-step process. First, BPG10 was aminated (NH_2-BPG10) by 1-ethyl-3-(3-(dimethylamino)propyl)carbodiimide/*N*-hydroxysuccinimide (EDC/NHS, Sigma) coupling with polyethylene glycol (PEG) diamine (~2 kDa, Sigma) in a 1:5 CS:diamine ratio and then purified *via* dialysis and lyophilized. Then, NH_2-BPG10 was reacted with 3,3′-dithiobis-(sulfosuccinimidyl propionate) (DTSSP, Sigma) to form disulfide bonds and then reduced with dithiothreitol (DTT, Sigma) to produce thiol-functionalized BPG10.

BPG10 Diffusion Model. Femoral condyles from adult bovine knee joints (n = 5, Research 87) were processed into 10 mm osteochondral plugs and equilibrated in 1× PBS at 4 °C overnight. Following equilibration, randomly selected plugs from each animal were incubated for 24 h with 2.5 mL of 10 mg/mL DCCH-BPG10 in 1× PBS, or in PBS alone as the control, following the previously established one-dimension (1D) diffusion model.[35] In brief, during the incubation, cartilage surface was placed downward to be in contact with the solution surface, while the underlying subchondral bone was clamped to a support. This setup minimized any direct contact of plug lateral sides with the solution, and thus, ensured that the diffusion takes place predominantly through the depth of cartilage tissue.[35] Following the incubation, articular cartilage was dissected, embedded in optimal cutting temperature (OCT) media, and unfixed, 8 μm thick sections were obtained *via* Kawamoto's film-assisted cryosectioning.[38] The sections were rinsed with 1× PBS to remove OCT and blocked with 10% goat serum (Life Technologies) for 20 min at room temperature. The sections were first fluorescently labeled with collagen VI primary antibody (70R-CR009X, Fitzgerald, 1:100 dilution) for 20 min, rinsed twice with 1× PBS for 5 min each, and then incubated with secondary antibody (goat antirabbit Alexa Fluor 488, AB150077, Abcam, 1:200 dilution) for 20 min in darkness. Sections were then rinsed twice for 5 min each with 1× PBS and mounted with FluorSave reagent (345789, EMD Millipore). For confocal microscopy, images were obtained using a Zeiss LSM 700 confocal microscope (Zeiss) at ex:405 nm for visualization of DCCH-BPG10 and ex:488 nm for collagen VI (repeated for $n \geq 5$ animals). Internal negative control was included following the same procedure but without the incubation of primary antibody.

Immunofluorescence-guided AFM Nanomechanical Mapping. Cryosections of adult bovine cartilage at ≈8 μm thickness in the sagittal plane were prepared in OCT media using Kawamoto's film-assisted method (n = 5 for each group).[38] The sections were first fluorescently labeled with collagen VI, following the same procedure described above. Samples were then tested using the total internal reflection fluorescence (TIRF) guided-AFM (MFP-3D, Asylum Research) in 1× PBS, following the established procedure.[9] To delineate the micromodulus of PCM and T-ECM, within each 20 × 20 μm^2 region of interest (ROI) with well-defined, ring-shaped PCM terrains, AFM nanomechanical mapping was performed in a 40 × 40 grid (1600 indentations) using polystyrene microspherical tips ($R \approx$ 2.25 μm, nominal $k \approx$ 0.6 N/m, HQ:NSC36/tipless/Cr–Au, cantilever C, NanoAndMore) up to ≈120 nN maximum indentation force at 10 μm/s rate (≥3–5 ROIs for each sample). To quantify the modulus of IT-ECM, nanomechanical mapping was performed on 20 × 20 μm^2 ROI with a 20 × 20 grid (400 indentations) in regions further removed from cells or PCM rings (≥5–7 ROIs for each sample). The effective indentation modulus, E_{ind}, was calculated by fitting the entire loading portion of the indentation force–depth (F–D) curve to the finite thickness-corrected Hertz Model.[69] Using corresponding IF images of collagen VI, we separated the E_{ind} of PCM and T-ECM using a custom MATLAB (Mathworks) program, and excluded values corresponding to cell remnants.

AFM Molecular Force Spectroscopy. Native aggrecan molecules were extracted from juvenile bovine cartilage *via* the 4 M guanidine hydrochloride method,[70] purified, and chemically end-functionalized with thiol-groups, following the established procedure.[42] We chemically end-attached thiol-functionalized aggrecan and thiol-functionalized BPG10 onto gold-coated planar silicon substrates or gold-coated microspherical colloidal tips ($R \approx$ 2.25 μm, AFM tip: Arrow-TL1Au, nominal $k \approx$ 0.03 N/m, NanoAndMore) *via* 48 h incubation in 1 mg/mL aggrecan or 1 mg/mL BPG10 aqueous

https://doi.org/10.1021/acsnano.1c09015
ACS Nano 2022, 16, 1220–1230

solutions, respectively. To assess the impact of free BPG10 or CS-GAG on aggrecan−aggrecan adhesion, the aggrecan-coated tip was programmed to compress the aggrecan-coated planar substrate at 1 μm/s rate up to ≈15 nN force, resulting in ≈50% molecular compressive strain of aggrecan. The tip was either immediately retracted (0 s dwell time) or held at the constant position for 20 s dwell time and then retracted from the surface at the same rate. For all experiments, from each pair of approach−retract force−distance curves, the maximum adhesion force, F_{ad} in (nN), and the total adhesion energy, E_{ad} (in fJ), were quantified ($n \geq 180$ measurements per condition from at least three experimental repeats).[42] The adhesion was measured in 1× PBS (without Ca^{2+}, Mg^{2+}), added with free BPG10 at 3.5 μg/mL, or CS-GAG at 3.3 μg/mL, and control with no BPG10 or CS-GAG added. The concentration of free CS-GAGs represented a molar equivalent of CS-GAGs on BPG10, and thus, ensured similar concentrations of CS-GAGs at the interfaces of two opposing aggrecan layers. To quantify BPG10−aggrecan molecular interactions under physiologic-like molecular packing, molecular adhesion was measured between (1) aggrecan-coated colloidal tips and BPG10-coated planar substrates, (2) BPG10-coated colloidal tips and aggrecan-coated substrates, and (3) BPG10-coated colloidal tips and BPG10-coated substrates, all in 1× PBS (without Ca^{2+}, Mg^{2+}), following the same molecular force spectroscopy experiment procedure at 0 and 20 s surface dwell time.

Intracellular Calcium Signaling ($[Ca^{2+}]_i$) and Cell Viability Assays. Cylindrical cartilage explants (4 mm diameter, 1 mm thickness) were harvested from fresh adult bovine knee joints (Research 87) at the controlled depth of ∼2 mm from the superficial layer. The plugs were cultured in chemically defined chondrogenic DMEM, 1% ITS+Premix, 50 μg/mL L-proline, 0.1 μM dexamethasone, 0.9 mM sodium pyruvate, 50 μg/mL ascorbate 2-phosphate), following the established procedure.[71] The cylindrical cartilage plugs were immersed in fresh DMEM with or without UV-sterilized BPG10 (1 mL of 4 mg/mL BPG10 in 1× PBS) for 24 h. Explant samples were then halved, with one half used for cell viability assay and the other half for spontaneous $[Ca^{2+}]_i$ signaling imaging.

Cell viability was assessed with a live/dead viability/cytotoxicity kit (L3224, Invitrogen) (≥6 explants from $n \geq 3$ animals for each group). For $[Ca^{2+}]_i$, halved cartilage plugs were incubated in Cal-520^{AM} (5 μM, AAT Bioquest) at 37 °C for 50 min, washed twice for 5 min each in phenol-red-free-DMEM (PRF-DMEM) and allowed to equilibrate for 15 min before imaging. Time-series of confocal $[Ca^{2+}]_i$ images were taken at 37 °C on the same group of cells every 1.5 s for 15 min using a LSM 700 laser scanning confocal microscope with a 20× objective (Zeiss) in isotonic (330 mOsm, ionic strength (IS) = 0.15 M), and then hypotonic (165 mOsm, IS = 0.075 M) PRF-DMEM. For each treatment condition and osmolarity, 100−120 chondrocytes in each field-of-view were analyzed, following the established procedure.[9] From the images of each ROI, we extracted the percentage of responding cells, $\%R_{cell}$, and for the cells that were responsive, the total number of $[Ca^{2+}]_i$ peaks, n_{peak}, during the 15 min observation period, and the average duration of peaks, t_{peak}. A total of ≥445 responsive cells from 9 explants per condition (from $n \geq 3$ animals) were analyzed for each group.

Statistical Analysis. To test the significance of BPG10 infiltration on cartilage micromodulus within each region, nonparametric Wilcoxon signed rank test was applied to compare the matched pairs of average micromodulus measured from each animal. For cell viability, n_{peak} and t_{peak}, given ≥445 cells were studied for each group, based on the central limit theorem, we applied the unpaired, two-sample *t*-test to test the significance of BPG10 infiltration or osmotic condition, followed by Holm−Bonferroni correction to adjust for family wise type I errors when applicable. For $\%R_{cell}$, the chi-squared test of proportions was applied, followed by Holm−Bonferroni correction. For F_{ad} and E_{ad} from molecular force spectroscopy, one-way ANOVA followed by Tukey−Kramer*posthoc* comparison was applied to detect differences between each group. In all the tests, the significance level was set at $\alpha = 0.05$.

AUTHOR INFORMATION

Corresponding Authors

Lin Han − *School of Biomedical Engineering, Science and Health Systems, Drexel University, Philadelphia, Pennsylvania 19104, United States;* orcid.org/0000-0003-4180-1288; Phone: (215) 571-3821; Email: lh535@drexel.edu; Fax: (215) 895-4983

Michele S. Marcolongo − *Department of Materials Science and Engineering, Drexel University, Philadelphia, Pennsylvania 19104, United States; Department of Mechanical Engineering, Villanova University, Villanova, Pennsylvania 19085, United States*; Phone: (610) 519-4940; Email: michele.marcolongo@villanova.edu; Fax: (215) 895-6760

Authors

Elizabeth R. Kahle − *School of Biomedical Engineering, Science and Health Systems, Drexel University, Philadelphia, Pennsylvania 19104, United States;* orcid.org/0000-0001-8394-459X

Biao Han − *School of Biomedical Engineering, Science and Health Systems, Drexel University, Philadelphia, Pennsylvania 19104, United States*

Prashant Chandrasekaran − *School of Biomedical Engineering, Science and Health Systems, Drexel University, Philadelphia, Pennsylvania 19104, United States*

Evan R. Phillips − *Department of Materials Science and Engineering, Drexel University, Philadelphia, Pennsylvania 19104, United States*

Mary K. Mulcahey − *Department of Orthopaedic Surgery, Tulane University School of Medicine, New Orleans, Louisiana 70112, United States*

X. Lucas Lu − *Department of Mechanical Engineering, University of Delaware, Newark, Delaware 19716, United States*

Complete contact information is available at: https://pubs.acs.org/10.1021/acsnano.1c09015

Notes

The authors declare no competing financial interest.

ACKNOWLEDGMENTS

This work was financially supported by the National Science Foundation (NSF) grant CMMI-1826202 (to M.S.M. and L.H.), Drexel Area of Research Excellence (DARE) Award (to M.S.M. and L.H.), National Institutes of Health (NIH) grant R01AR074490 (to L.H.) and R01AR074472 (to X.L.L.), as well as NIH Grant P30AR069619 to the Penn Center for Musculoskeletal Disorders. We thank the Singh Center for Nanotechnology at the University of Pennsylvania for the use of TIRF MFP-3D, which is part of the National Nanotechnology Coordinated Infrastructure Program supported by the NSF grant NNCI-1542153. We thank Dr. K. Prudnikova (Drexel University) for the design and synthesis of BPG10, as well as Dr. D. R. Chery (Drexel University) for insightful discussions. All imaging was performed at Drexel University's Cell Imaging Center.

REFERENCES

(1) Wang, N.; Tytell, J. D.; Ingber, D. E. Mechanotransduction at a Distance: Mechanically Coupling the Extracellular Matrix with the Nucleus. *Nat. Rev. Mol. Cell Biol.* **2009**, *10*, 75−82.

(2) Brassart-Pasco, S.; Brézillon, S.; Brassart, B.; Ramont, L.; Oudart, J. B.; Monboisse, J. C. Tumor Microenvironment: Extracellular Matrix Alterations Influence Tumor Progression. *Front. Oncol.* **2020**, *10*, 397.
(3) Gattazzo, F.; Urciuolo, A.; Bonaldo, P. Extracellular Matrix: A Dynamic Microenvironment for Stem Cell Niche. *Biochim. Biophys. Acta* **2014**, *1840*, 2506−2519.
(4) Yamagata, M.; Saga, S.; Kato, M.; Bernfield, M.; Kimata, K. Selective Distributions of Proteoglycans and Their Ligands in Pericellular Matrix of Cultured Fibroblasts. Implications for Their Roles in Cell-Substratum Adhesion. *J. Cell Sci.* **1993**, *106*, 55−65.
(5) Evanko, S. P.; Angello, J. C.; Wight, T. N. Formation of Hyaluronan- and Versican-Rich Pericellular Matrix Is Required for Proliferation and Migration of Vascular Smooth Muscle Cells. *Arterioscler. Thromb. Vasc. Biol.* **1999**, *19*, 1004−1013.
(6) Wang, B.; Lai, X.; Price, C.; Thompson, W. R.; Li, W.; Quabili, T. R.; Tseng, W. J.; Liu, X. S.; Zhang, H.; Pan, J.; Kirn-Safran, C. B.; Farach-Carson, M. C.; Wang, L. Perlecan-Containing Pericellular Matrix Regulates Solute Transport and Mechanosensing within the Osteocyte Lacunar-Canalicular System. *J. Bone Miner. Res.* **2014**, *29*, 878−891.
(7) Han, Y.; Cowin, S. C.; Schaffler, M. B.; Weinbaum, S. Mechanotransduction and Strain Amplification in Osteocyte Cell Processes. *Proc. Natl. Acad. Sci. U. S. A.* **2004**, *101*, 16689−16694.
(8) Paszek, M. J.; DuFort, C. C.; Rossier, O.; Bainer, R.; Mouw, J. K.; Godula, K.; Hudak, J. E.; Lakins, J. N.; Wijekoon, A. C.; Cassereau, L.; Rubashkin, M. G.; Magbanua, M. J.; Thorn, K. S.; Davidson, M. W.; Rugo, H. S.; Park, J. W.; Hammer, D. A.; Giannone, G.; Bertozzi, C. R.; Weaver, V. M. The Cancer Glycocalyx Mechanically Primes Integrin-Mediated Growth and Survival. *Nature* **2014**, *511*, 319−325.
(9) Chery, D. R.; Han, B.; Li, Q.; Zhou, Y.; Heo, S. J.; Kwok, B.; Chandrasekaran, P.; Wang, C.; Qin, L.; Lu, X. L.; Kong, D.; Enomoto-Iwamoto, M.; Mauck, R. L.; Han, L. Early Changes in Cartilage Pericellular Matrix Micromechanobiology Portend the Onset of Post-Traumatic Osteoarthritis. *Acta Biomater.* **2020**, *111*, 267−278.
(10) Guilak, F.; Nims, R. J.; Dicks, A.; Wu, C. L.; Meulenbelt, I. Osteoarthritis as a Disease of the Cartilage Pericellular Matrix. *Matrix Biol.* **2018**, *71*−*72*, 40−50.
(11) Henke, E.; Nandigama, R.; Ergün, S. Extracellular Matrix in the Tumor Microenvironment and Its Impact on Cancer Therapy. *Front. Mol. Biosci.* **2020**, *6*, 160.
(12) Wilusz, R. E.; Sanchez-Adams, J.; Guilak, F. The Structure and Function of the Pericellular Matrix of Articular Cartilage. *Matrix Biol.* **2014**, *39*, 25−32.
(13) Sanchez-Adams, J.; Wilusz, R. E.; Guilak, F. Atomic Force Microscopy Reveals Regional Variations in the Micromechanical Properties of the Pericellular and Extracellular Matrices of the Meniscus. *J. Orthop. Res.* **2013**, *31*, 1218−1225.
(14) Cao, L.; Guilak, F.; Setton, L. A. Three-Dimensional Morphology of the Pericellular Matrix of Intervertebral Disc Cells in the Rat. *J. Anat.* **2007**, *211*, 444−452.
(15) Scott, A.; Cook, J. L.; Hart, D. A.; Walker, D. C.; Duronio, V.; Khan, K. M. Tenocyte Responses to Mechanical Loading *in Vivo*: A Role for Local Insulin-Like Growth Factor 1 Signaling in Early Tendinosis in Rats. *Arthritis Rheumatol.* **2007**, *56*, 871−881.
(16) Reitsma, S.; Slaaf, D. W.; Vink, H.; van Zandvoort, M. A.; oude Egbrink, M. G. The Endothelial Glycocalyx: Composition, Functions, and Visualization. *Pflugers Arch.* **2007**, *454*, 345−359.
(17) Ferreira, S. A.; Motwani, M. S.; Faull, P. A.; Seymour, A. J.; Yu, T. T. L.; Enayati, M.; Taheem, D. K.; Salzlechner, C.; Haghighi, T.; Kania, E. M.; et al. Bi-Directional Cell-Pericellular Matrix Interactions Direct Stem Cell Fate. *Nat. Commun.* **2018**, *9*, 4049.
(18) Möckl, L. The Emerging Role of the Mammalian Glycocalyx in Functional Membrane Organization and Immune System Regulation. *Front. Cell Dev. Biol.* **2020**, *8*, 253.
(19) Karamanos, N. K.; Piperigkou, Z.; Theocharis, A. D.; Watanabe, H.; Franchi, M.; Baud, S.; Brézillon, S.; Götte, M.; Passi, A.; Vigetti, D.; Ricard-Blum, S.; Sanderson, R. D.; Neill, T.; Iozzo, R. V. Proteoglycan Chemical Diversity Drives Multifunctional Cell Regulation and Therapeutics. *Chem. Rev.* **2018**, *118*, 9152−9232.
(20) Guilak, F.; Alexopoulos, L. G.; Upton, M. L.; Youn, I.; Choi, J. B.; Cao, L.; Setton, L. A.; Haider, M. A. The Pericellular Matrix as a Transducer of Biomechanical and Biochemical Signals in Articular Cartilage. *Ann. N. Y. Acad. Sci.* **2006**, *1068*, 498−512.
(21) Lark, M. W.; Bayne, E. K.; Lohmander, L. S. Aggrecan Degradation in Osteoarthritis and Rheumatoid Arthritis. *Acta Orthop. Scand.* **1995**, *66*, 92−97.
(22) Walimbe, T.; Panitch, A. Proteoglycans in Biomedicine: Resurgence of an Underexploited Class of ECM Molecules. *Front. Pharmacol.* **2020**, *10*, 1661.
(23) Poole, C. A.; Ayad, S.; Schofield, J. R. Chondrons from Articular Cartilage: I. Immunolocalization of Type VI Collagen in the Pericellular Capsule of Isolated Canine Tibial Chondrons. *J. Cell Sci.* **1988**, *90*, 635−643.
(24) SundarRaj, N.; Fite, D.; Ledbetter, S.; Chakravarti, S.; Hassell, J. R. Perlecan Is a Component of Cartilage Matrix and Promotes Chondrocyte Attachment. *J. Cell Sci.* **1995**, *108*, 2663−2672.
(25) Kavanagh, E.; Ashhurst, D. E. Development and Aging of the Articular Cartilage of the Rabbit Knee Joint: Distribution of Biglycan, Decorin, and Matrilin-1. *J. Histochem. Cytochem.* **1999**, *47*, 1603−1616.
(26) Poole, A. R.; Pidoux, I.; Reiner, A.; Rosenberg, L. An Immunoelectron Microscope Study of the Organization of Proteoglycan Monomer, Link Protein, and Collagen in the Matrix of Articular Cartilage. *J. Cell Biol.* **1982**, *93*, 921−937.
(27) Quinn, T. M.; Maung, A. A.; Grodzinsky, A. J.; Hunziker, E. B.; Sandy, J. D. Physical and Biological Regulation of Proteoglycan Turnover Around Chondrocytes in Cartilage Explants. Implications for Tissue Degradation and Repair. *Ann. N. Y. Acad. Sci.* **1999**, *878*, 420−441.
(28) Bayliss, M. T.; Howat, S.; Davidson, C.; Dudhia, J. The Organization of Aggrecan in Human Articular Cartilage. Evidence for Age-Related Changes in the Rate of Aggregation of Newly Synthesized Molecules. *J. Biol. Chem.* **2000**, *275*, 6321−6327.
(29) Han, L.; Grodzinsky, A. J.; Ortiz, C. Nanomechanics of the Cartilage Extracellular Matrix. *Annu. Rev. Mater. Res.* **2011**, *41*, 133−168.
(30) Chery, D. R.; Han, B.; Zhou, Y.; Wang, C.; Adams, S. M.; Chandrasekaran, P.; Kwok, B.; Heo, S.-J.; Enomoto-Iwamoto, M.; Lu, X. L.; Kong, D.; Iozzo, R. V.; Birk, D. E.; Mauck, R. L.; Han, L. Decorin Regulates Cartilage Pericellular Matrix Micromechanobiology. *Matrix Biol.* **2021**, *96*, 1−17.
(31) Prudnikova, K.; Yucha, R. W.; Patel, P.; Kriete, A. S.; Han, L.; Penn, L. S.; Marcolongo, M. S. Biomimetic Proteoglycans Mimic Macromolecular Architecture and Water Uptake of Natural Proteoglycans. *Biomacromolecules* **2017**, *18*, 1713−1723.
(32) Prudnikova, K.; Lightfoot Vidal, S. E.; Sarkar, S.; Yu, T.; Yucha, R. W.; Ganesh, N.; Penn, L. S.; Han, L.; Schauer, C. L.; Vresilovic, E. J.; Marcolongo, M. S. Aggrecan-Like Biomimetic Proteoglycans (BPGs) Composed of Natural Chondroitin Sulfate Bristles Grafted onto a Poly(Acrylic Acid) Core for Molecular Engineering of the Extracellular Matrix. *Acta Biomater.* **2018**, *75*, 93−104.
(33) Sarkar, S.; Moorehead, C.; Prudnikova, K.; Schauer, C. L.; Penn, L. S.; Marcolongo, M. Synthesis of Macromolecular Mimics of Small Leucine-Rich Proteoglycans with a Poly(Ethylene Glycol) Core and Chondroitin Sulphate Bristles. *Carbohydr. Polym.* **2017**, *166*, 338−347.
(34) Phillips, E. R.; Prudnikova, K.; Bui, T.; Taylor, A. J.; Galindo, D. A.; Huneke, R. B.; Hou, J. S.; Mulcahey, M. K.; Marcolongo, M. S. Biomimetic Proteoglycans Can Molecularly Engineer Early Osteoarthritic Cartilage *in Vivo*. *J. Orthop. Res.* **2019**, *37*, 403−411.
(35) Phillips, E. R.; Haislup, B. D.; Bertha, N.; Lefchak, M.; Sincavage, J.; Prudnikova, K.; Shallop, B.; Mulcahey, M. K.; Marcolongo, M. S. Biomimetic Proteoglycans Diffuse Throughout Articular Cartilage and Localize within the Pericellular Matrix. *J. Biomed. Mater. Res., Part A* **2019**, *107*, 1977−1987.

https://doi.org/10.1021/acsnano.1c09015
ACS Nano 2022, 16, 1220−1230

(36) Ng, L.; Grodzinsky, A. J.; Patwari, P.; Sandy, J.; Plaas, A.; Ortiz, C. Individual Cartilage Aggrecan Macromolecules and Their Constituent Glycosaminoglycans Visualized *via* Atomic Force Microscopy. *J. Struct. Biol.* **2003**, *143*, 242−257.
(37) Darling, E. M.; Wilusz, R. E.; Bolognesi, M. P.; Zauscher, S.; Guilak, F. Spatial Mapping of the Biomechanical Properties of the Pericellular Matrix of Articular Cartilage Measured *in Situ via* Atomic Force Microscopy. *Biophys. J.* **2010**, *98*, 2848−2856.
(38) Kawamoto, T.; Kawamoto, K. Preparation of Thin Frozen Sections from Nonfixed and Undecalcified Hard Tissues Using Kawamot's Film Method. *Methods Mol. Biol.* **2014**, *1130*, 149−164.
(39) Chao, P. H.; West, A. C.; Hung, C. T. Chondrocyte Intracellular Calcium, Cytoskeletal Organization, and Gene Expression Responses to Dynamic Osmotic Loading. *Am. J. Physiol. Cell Physiol.* **2006**, *291*, C718−725.
(40) Hing, W.A; Sherwin, A.F; Ross, J.M; Poole, C.A The Influence of the Pericellular Microenvironment on the Chondrocyte Response to Osmotic Challenge. *Osteoarthr. Cartil.* **2002**, *10*, 297−307.
(41) Wight, T. N.; Heinegård, D. K.; Hascall, V. C.*Cell Biology of Extracellular Matrix*; Plenum Press: New York, 1991.
(42) Han, L.; Dean, D.; Daher, L. A.; Grodzinsky, A. J.; Ortiz, C. Cartilage Aggrecan Can Undergo Self-Adhesion. *Biophys. J.* **2008**, *95*, 4862−4870.
(43) Rojas, F. P.; Batista, M. A.; Lindburg, C. A.; Dean, D.; Grodzinsky, A. J.; Ortiz, C.; Han, L. Molecular Adhesion between Cartilage Extracellular Matrix Macromolecules. *Biomacromolecules* **2014**, *15*, 772−780.
(44) Wang, T.; Lai, J. H.; Yang, F. Effects of Hydrogel Stiffness and Extracellular Compositions on Modulating Cartilage Regeneration by Mixed Populations of Stem Cells and Chondrocytes *in Vivo*. *Tissue Eng. Part A* **2016**, *22*, 1348−1356.
(45) Wilusz, R. E.; Zauscher, S.; Guilak, F. Micromechanical Mapping of Early Osteoarthritic Changes in the Pericellular Matrix of Human Articular Cartilage. *Osteoarthr. Cartil.* **2013**, *21*, 1895−1903.
(46) Weber, J. F.; Waldman, S. D. Calcium Signaling as a Novel Method to Optimize the Biosynthetic Response of Chondrocytes to Dynamic Mechanical Loading. *Biomech. Model. Mechanobiol.* **2014**, *13*, 1387−1397.
(47) Doyran, B.; Tong, W.; Li, Q.; Jia, H.; Zhang, X.; Chen, C.; Enomoto-Iwamoto, M.; Lu, X. L.; Qin, L.; Han, L. Nanoindentation Modulus of Murine Cartilage: A Sensitive Indicator of the Initiation and Progression of Post-Traumatic Osteoarthritis. *Osteoarthr. Cartil.* **2017**, *25*, 108−117.
(48) Lee, W.; Nims, R. J.; Savadipour, A.; Zhang, Q.; Leddy, H. A.; Liu, F.; McNulty, A. L.; Chen, Y.; Guilak, F.; Liedtke, W. B. Inflammatory Signaling Sensitizes Piezo1 Mechanotransduction In Articular Chondrocytes as a Pathogenic Feed-Forward Mechanism in Osteoarthritis. *Proc. Natl. Acad. Sci. U. S. A.* **2021**, *118*, No. e2001611118.
(49) Buschmann, M. D.; Grodzinsky, A. J. A Molecular Model of Proteoglycan-Associated Electrostatic Forces in Cartilage Mechanics. *J. Biomech. Eng.* **1995**, *117*, 179−192.
(50) Dean, D.; Seog, J.; Ortiz, C.; Grodzinsky, A. J. Molecular-Level Theoretical Model for Electrostatic Interactions within Polyelectrolyte Brushes: Applications to Charged Glycosaminoglycans. *Langmuir* **2003**, *19*, 5526−5539.
(51) Dean, D.; Han, L.; Grodzinsky, A. J.; Ortiz, C. Compressive Nanomechanics of Opposing Aggrecan Macromolecules. *J. Biomech.* **2006**, *39*, 2555−2565.
(52) Han, B.; Li, Q.; Wang, C.; Patel, P.; Adams, S. M.; Doyran, B.; Nia, H. T.; Oftadeh, R.; Zhou, S.; Li, C. Y.; Liu, X. S.; Lu, X. L.; Enomoto-Iwamoto, M.; Qin, L.; Mauck, R. L.; Iozzo, R. V.; Birk, D. E.; Han, L. Decorin Regulates the Aggrecan Network Integrity and Biomechanical Functions of Cartilage Extracellular Matrix. *ACS Nano* **2019**, *13*, 11320−11333.
(53) Seog, J.; Dean, D.; Rolauffs, B.; Wu, T.; Genzer, J.; Plaas, A. H.; Grodzinsky, A. J.; Ortiz, C. Nanomechanics of Opposing Glycosaminoglycan Macromolecules. *J. Biomech.* **2005**, *38*, 1789−1797.
(54) Voiutskii, S. S.*Autohesion and Adhesion of High Polymers*; John Wiley & Sons: Hoboken, NJ, 1963.
(55) Williamson, A. K.; Chen, A. C.; Sah, R. L. Compressive Properties and Function-Composition Relationships of Developing Bovine Articular Cartilage. *J. Orthop. Res.* **2001**, *19*, 1113−1121.
(56) Stuart, K.; Paderi, J.; Snyder, P. W.; Freeman, L.; Panitch, A. Collagen-Binding Peptidoglycans Inhibit MMP Mediated Collagen Degradation and Reduce Dermal Scarring. *PLoS One* **2011**, *6*, No. e22139.
(57) Bernhard, J. C.; Panitch, A. Synthesis and Characterization of an Aggrecan Mimic. *Acta Biomater.* **2012**, *8*, 1543−1550.
(58) Sharma, S.; Vazquez-Portalatin, N.; Calve, S.; Panitch, A. Biomimetic Molecules Lower Catabolic Expression and Prevent Chondroitin Sulfate Degradation in an Osteoarthritic *ex Vivo* Model. *ACS Biomater. Sci. Eng.* **2016**, *2*, 241−250.
(59) Iozzo, R. V. Perlecan: A Gem of a Proteoglycan. *Matrix Biol.* **1994**, *14*, 203−208.
(60) Melrose, J.; Roughley, P.; Knox, S.; Smith, S.; Lord, M.; Whitelock, J. The Structure, Location, and Function of Perlecan, a Prominent Pericellular Proteoglycan of Fetal, Postnatal, and Mature Hyaline Cartilages. *J. Biol. Chem.* **2006**, *281*, 36905−36914.
(61) Vincent, T. L.; McLean, C. J.; Full, L. E.; Peston, D.; Saklatvala, J. FGF-2 is Bound to Perlecan in the Pericellular Matrix of Articular Cartilage, Where It Acts as a Chondrocyte Mechanotransducer. *Osteoarthr. Cartil.* **2007**, *15*, 752−763.
(62) Hua, Q.; Knudson, C. B.; Knudson, W. Internalization of Hyaluronan by Chondrocytes Occurs *via* Receptor-Mediated Endocytosis. *J. Cell Sci.* **1993**, *106*, 365−375.
(63) Danielson, B. T.; Knudson, C. B.; Knudson, W. Extracellular Processing of the Cartilage Proteoglycan Aggregate and Its Effect on CD44-Mediated Internalization of Hyaluronan. *J. Biol. Chem.* **2015**, *290*, 9555−9570.
(64) Jin, T.; Wu, D.; Liu, X. M.; Xu, J. T.; Ma, B. J.; Ji, Y.; Jin, Y. Y.; Wu, S. Y.; Wu, T.; Ma, K. Intra-Articular Delivery of Celastrol by Hollow Mesoporous Silica Nanoparticles for pH-Sensitive Anti-Inflammatory Therapy Against Knee Osteoarthritis. *J. Nanobiotechnol.* **2020**, *18*, 94.
(65) Yao, Q.; Kou, L.; Tu, Y.; Zhu, L. MMP-Responsive 'Smart' Drug Delivery and Tumor Targeting. *Trends Pharmacol. Sci.* **2018**, *39*, 766−781.
(66) Bayliss, M. T.; Osborne, D.; Woodhouse, S.; Davidson, C. Sulfation of Chondroitin Sulfate in Human Articular Cartilage. The Effect of Age, Topographical Position, and Zone of Cartilage on Tissue Composition. *J. Biol. Chem.* **1999**, *274*, 15892−15900.
(67) Pratta, M. A.; Tortorella, M. D.; Arner, E. C. Age-Related Changes in Aggrecan Glycosylation Affect Cleavage by Aggrecanase. *J. Biol. Chem.* **2000**, *275*, 39096−39102.
(68) Lee, H.-Y.; Han, L.; Roughley, P. J.; Grodzinsky, A. J.; Ortiz, C. Age-Related Nanostructural and Nanomechanical Changes of Individual Human Cartilage Aggrecan Monomers and Their Glycosaminoglycan Side Chains. *J. Struct. Biol.* **2013**, *181*, 264−273.
(69) Dimitriadis, E. K.; Horkay, F.; Maresca, J.; Kachar, B.; Chadwick, R. S. Determination of Elastic Moduli of Thin Layers of Soft Material Using the Atomic Force Microscope. *Biophys. J.* **2002**, *82*, 2798−2810.
(70) Roughley, P. J.; White, R. Age-Related Changes in the Structure of the Proteoglycan Subunits from Human Articular Cartilage. *J. Biol. Chem.* **1980**, *255*, 217−224.
(71) Zhou, Y.; David, M. A.; Chen, X.; Wan, L. Q.; Duncan, R. L.; Wang, L.; Lu, X. L. Effects of Osmolarity on the Spontaneous Calcium Signaling of *in Situ* Juvenile and Adult Articular Chondrocytes. *Ann. Biomed. Eng.* **2016**, *44*, 1138−1147.

https://doi.org/10.1021/acsnano.1c09015
ACS Nano 2022, 16, 1220−1230